Multiscale Extended Finite Element Method for Modelling Mechanical Deformation in Porous Media with Propagating Fractures

Xu, F.; Hajibeygi, H.; Sluys, B.

DOI
10.3997/2214-4609.202244025

Publication date
2022

Document Version
Final published version

Published in
European Conference on the Mathematics of Geological Reservoirs 2022, ECMOR 2022

ECMOR 2022
European Conference on the Mathematics of Geological Reservoirs

EAGE

Multiscale Extended Finite Element Method for Modelling Mechanical Deformation in Porous Media with Propagating Fractures

F. Xu[1], H. Hajibeygi[1], B. Sluys[1]

[1] Delft University of Technology

Summary

Altering the state of the stress of the subsurface reservoirs can lead fractures to slip and extend their lengths (i.e., to propagate). This process can even be engineered, in many applications, e.g., enhanced geothermal systems. As such, accurate and efficient simulation of the mechanical deformation of the subsurface geological reservoirs, allowing for fracture propagation, is at the core of many geoscientific operational designs.

Subsurface reservoirs entail many fractures at multiple scales. Implementation of 3D complex grids on these complex fractured systems, for mechanical deformation analyses, is extremely challenging. An alternative approach can be developed by using extended finite element methods (XFEM). XFEM allows for capturing the fractures effects on a conveniently-generated structured matrix mesh. The cracks are introduced by extra degrees of freedom (DOFs) on the nodes of the matrix rock mesh. For geoscientific applications, however, XFEM results in too many DOFs which are beyond the scope of simulators. Additionally, for propagating fractures, these DOFs need to be updated in response to the dynamic extension of the fractures in the domain. The propagation process not only adds to the sensitivity of the outputs to the accuracy of the estimated stress field, but also increases the size of the linear systems. In addition to these, matrix rocks are often highly heterogeneous, at high resolutions.

In this work, we present a novel multiscale procedure for propagating fractures in heterogeneous geological reservoirs. For the first time in the community, we present the highly fractured systems at coarser resolutions via XFEM-based basis functions, which also account for the propagating effects. Fractures are allowed to extend their scale and the enriched basis functions are locally updated. Using these bases, the coarse scale system is obtained in which no extra DOFs due to fractures exist. This significantly reduces the computational complexity.

As a significant step forward compared with our recently-published journal paper [Xu, Hajibeygi, Sluys, Journal of Computational Physics, 2021], in this conference contribution we allow the fractures to propagate. Specially, we introduce a local-global-based approach, in which fracture propagation is treated only at local stage; while the stress and deformation are modelled at global scale. In the search of convenient implementation, the procedure is presented algebraically.

Through several test cases, we demonstrate the applicability of the method for complex fractured media. Specially we demonstrate that propagation can be modeled at local scale, while accurate stress and deformation fields are obtained at global scale.

Introduction

The equilibrium state of fractured geological formations may be violated due to a sudden change of the state of stress, which can arise from anthropological operations. As a consequence, fractures can be activated and slide or even grow (i.e., propagate). The consequences of the sliding fracture phenomena can be disastrous. To be able to control and alleviate these risks, accurate and efficient simulation of growing fractures in underground formations is crucial.

In view of fracture growth, some mechanical theories have been proposed in the literature. In Griffith's theory [(20)], the fracture grows when the energy release rate at its tip is larger than or equal to a prescribed critical value, which is a material dependent parameter. A few classical theories have been applied to further track the growth direction. The maximum principle stress theory (16) has been proved to be able to track the direction of crack growth accurately. The maximum energy release rate (45; 38) allows to predict crack growth for both tension and compression scenarios, which makes it appealing for practical geoscience applications.

To simulate growing fractures, the extended finite element method (XFEM) (6; 33), which is an embedded method for fracture mechanics simulation, is a viable option. Unlike the unstructured grid approach (36; 7; 27; 18; 44), XFEM implies the enrichment to shape functions meanwhile not interfering with the discretization layout. Therefore, independent meshes can be assigned to the matrix and fractures (24; 42; 29; 15; 46). To match the partition of unity (PoU) property of shape functions (32), extra degrees of freedom (DOFs) are given to enriched nodes. Considering different geometric relationships between fractures and elements, two types of enrichment can be applied: jump enrichment and junction enrichment (33; 5; 4; 31; 13). Level set functions are introduced to help XFEM track the fracture tip positions (34; 40; 8).

In underground fractured formations, heterogeneity that spans over larger length scales need to be considered together with fractures of different length-scales. The classical XFEM is not readily applicable in the geoscience community due to the large number of extra DOFs for highly fractured formations. Note that possible model-order-reduction schemes, such as upscaling or homogenization, are not able to capture the detailed sharp gradients in stress and strain nearby the fractures (2; 1; 3; 25; 30; 48; 35; 28; 21). Alternatively, the multiscale method (MS) (23; 10; 39; 26; 14; 37; 9; 17; 19; 22; 43; 12) has been proved to be able to capture the fine-scale heterogeneity, yet construct accurate coarse-scale systems and thus reduce the computational costs. In presence of fractures, the multiscale extended finite element method (MS-XFEM) has been recently developed by Xu et al. (47). This method incorporates the fine scale discontinuities into the basis functions and creates finite element type problem on the coarse-scale mesh which contains no extra DOFs. The generation of basis functions can be done algebraically as stated in (47) conveniently. To control the quality of final results to a controlled level, the iterative method is applied.

This paper develops an iterative MS-XFEM (iMS-XFEM) to simulate fracture growth in highly fractured formations. The growth of fractures are tracked using level set functions. The growing fracture tips are tracked by updating the basis functions which are generated based on the revised fine-scale stiffness matrix in an algebraic manner. Thus, in each time step the basis functions are updated only at the local domains in which the fracture geometry will change. Still, no extra DOFs are introduced on the coarse scale system. Preconditioned GMRES is used during the iterative solving stage to control the accuracy of the final results.

The structure of this paper is set as follows. First, the governing equations and the fine scale XFEM method are introduced. Next, fracture growth simulation using fine scale XFEM is introduced, followed by the fine scale XFEM in simulating multiple fractures propagation. Then the principles of how iMS-XFEM in a multiple cracks simulation is presented.

Governing Equations and XFEM

Consider a domain Ω bounded by Γ as shown in Fig. 1. Prescribed displacements or Dirichlet boundary condition are imposed on Γ_u, while traction are imposed on Γ_t. The multiple crack surfaces $\Gamma_{c,i=1...n}$ (lines in 2-D and surfaces in 3-D) are assumed to be traction-free.

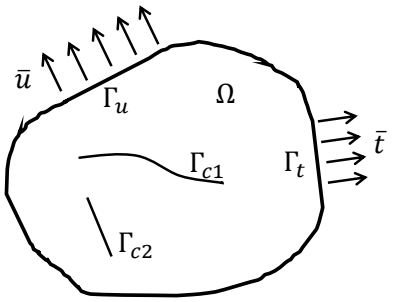

Figure 1: An illustration of fractured domain setup.

The momentum balance equations and boundary conditions read

$$\nabla \cdot \sigma + f = 0 \quad in\ \Omega, \tag{1}$$
$$\sigma \cdot \vec{n} = \bar{t} \quad on\ \Gamma_t, \tag{2}$$
$$\sigma \cdot \vec{n} = 0 \quad on\ \Gamma_c, \tag{3}$$
$$u = \bar{u} \quad on\ \Gamma_u, \tag{4}$$

where σ is the stress tensor and u is the displacement field over the whole domain. $\vec{n}$ is the normal vector pointing outside the domain.
A linear elastic constitutive law is applied in this paper. The second order partial differential equation (PDE) for displacement field u reads

$$\nabla \cdot (\mathbf{C} : \nabla^s u) + f = 0, \tag{5}$$

where $\mathbf{C}$ is the linear elastic constitutive tensor. Eq. (5) is then solved for computational domains with cracks (representing faults and fractures). This is done by using XFEM. Next, the XFEM is revisited briefly.

Extended Finite Element Method (XFEM)

In this paper, two types of enrichment, jump enrichment and junction enrichment, are introduced to represent discontinuities. The jump enrichment represents the discontinuity in the displacement field across the fractured body. The jump enrichment is often chosen as a step function, which can be expressed as

$$H(x) = \begin{cases} 1 \\ -1 \end{cases} .$$

To simulate the crossing of fractures in XFEM, the junction enrichment, or the crossing enrichment, is applied. There are two situations of crossing considered: T-shape crossing and X-shape crossing and the details of these two functions can be referred into (13). The junction functions values distribution inside crossing cracked element are plotted in Fig. 2.

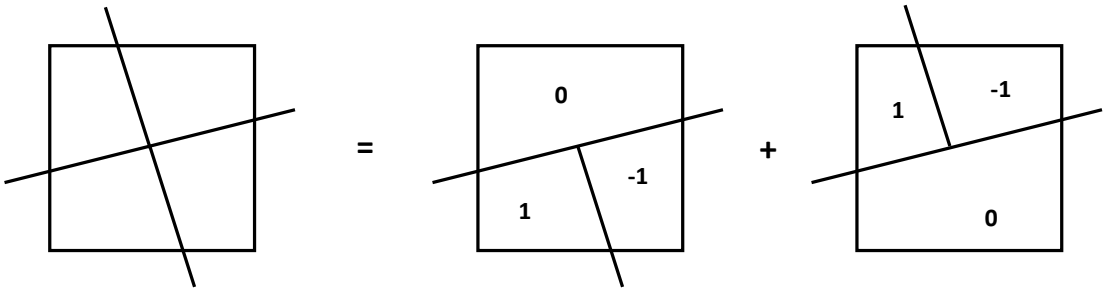

Figure 2: Two types of the junction enrichment functions. X-shape junction enrichment can be divided into two T-shape enrichment functions.

The displacement field u at fine-scale resolution h by u^h is as

$$u \approx u^h = \sum_{i \in \Omega^h} u_i N_i + \sum_{j \in J} a_j N_j H(x) + \sum_{m \in M} b_m N_m J(x), \tag{6}$$

where N, H and J represent, respectively, the classical FEM shape functions, the jump function and the junction enrichment functions. u denotes the standard DOFs associated to the classical finite element method and a denotes the extra DOFs associated to the jump enriched nodes. Note that a also includes the jump enrichment related extra DOFs due to the main crack in the junction enriched element. The multipliers b are the extra DOFs due to the junction enrichment. The resulting linear system entails the nodal displacement unknowns u, as well as the jump enriched extra DOFs a and junction enriched extra DOFs b per fracture (and fault). The augmented XFEM linear system $K^h\, d^h = f^h$, therefore, reads

$$\underbrace{\begin{bmatrix} K_{uu} & K_{ua} & K_{ub} \\ K_{au} & K_{aa} & K_{ab} \\ K_{bu} & K_{ba} & K_{bb} \end{bmatrix}}_{\mathbf{K^h}} \underbrace{\begin{bmatrix} u \\ a \\ b \end{bmatrix}}_{\mathbf{d^h}} = \underbrace{\begin{bmatrix} f_u \\ f_a \\ f_b \end{bmatrix}}_{\mathbf{f^h}}. \tag{7}$$

It is clear that additional blocks are added compared to the classical FEM stiffness matrix. Although the complicated meshing procedure is avoided, application of the XFEM in geoscience field simulations is still a nontrivial task. With the presence of highly fractured formations, the size of these additional blocks becomes too big to be resolved by state-of-the-art simulators. To resolve this challenge, a multi-scale simulation strategy is introduced in this paper.

Multiple Fractures Propagation Simulation Using XFEM

As mentioned, the use of a multiscale method enables a more feasible application of XFEM into a highly fractured formations simulation. However, in this section, a method for fractures growth using only fine scale XFEM is introduced. In this section this method will be expanded to the multiscale extended finite element method (MS-XFEM) which can be used for highly fractured systems.

Propagation criterion

Griffith's theory (20) states that the fracture tip will grow if the energy release rate, G, is larger than or equal to the critical energy release rate, G_c. This is expressed as

$$G \geqslant G_c, \tag{8}$$

where G is defined as the rate of energy decreased per unit fracture surface area increased (20). Eq. (8) can be also written in terms of the stress intensity factor K as

$$K \geqslant K_c, \tag{9}$$

where K_c is called fracture toughness.
The fracture increment is usually defined as a constant during each time step. The fracture angle of the propagation crack tip can be quantified using different theories. In this paper, only test cases under tensile forces are performed, the maximum principle stress theory is used to predict the direction of fracture propagation according to

$$\theta = 2\arctan\frac{1}{4}(\frac{K_I}{K_{II}} \pm \sqrt{(\frac{K_I}{K_{II}})^2 + 8}), \tag{10}$$

where K_I is the stress intensity factor for mode I and K_{II} is the stress intensity factor for mode II.

Multiple fractures propagation

Unlike propagation of a single fracture, the impact of the increment of one fracture tip to another needs also to be considered in a multiple fractures propagation problem. Some fracture tips may grow and they are grouped in the algorithm as competitive tips n_{comp}. These tips must strictly follow Eq. (9). But not all of them can grow since the whole fractured system tend to release the minimum global energy to reach a new equilibrium state (41). The unstable configuration of fractures path is defined as

$$(\frac{\partial G_i}{\partial l_j} - \frac{\partial G_{c,i}}{\partial l_j}) \geqslant 0, \quad \forall i, j \in n_{comp}, \tag{11}$$

where $\partial G_i/\partial l_j$ is the derivative of energy release rate of crack tip i with respect to crack tip j increment. $\partial G_{c,i}/\partial l_j$ is the derivative of critical energy release rate of crack tip i with respect to crack tip j increment.
At the beginning of each fracture growth step, the matrix $\partial G/\partial l$ needs to be constructed to check whether the chosen growing path meets the criterion described by Eq. (11). The double virtual incremental method is applied (41; 8) to construct the matrix $\partial G/\partial l$. In the double virtual incremental method, it is assumed that the growth of the tips would only affect a small region near the fractures tips. The virtual fracture tip i increment, l_i, is approximated using virtual displacement function Θ_i. The virtual fracture tip j increment, l_j, is approximated using the virtual displacement function Π_j. These functions are shown in Fig. 3.

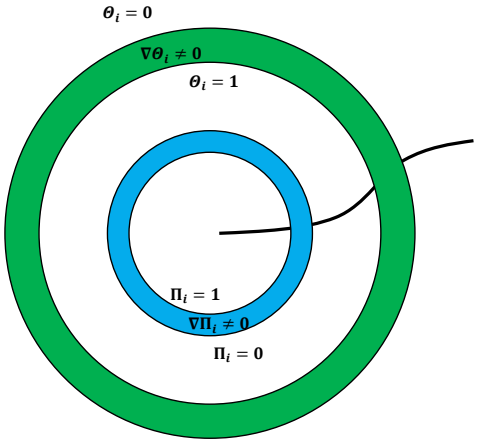

Figure 3: Function Π (green) and function Θ (blue) at fracture tip. The gradients of both functions are 0 outside the colored zones.

Note that the radius of the non-zero gradient zone of function Π is normally twice the radius of the none-zero gradient zone of function Θ. These two zones are not allowed to intersect.
The virtual displacement field $\tilde{\mathbf{d}}_j$ is constructed in order to compute $\partial G_i/\partial l_j$. To compute this virtual

displacement field, a virtual force vector $\tilde{\mathbf{f}}_{\Pi_j}$ around the fracture tip j is defined as

$$\tilde{\mathbf{f}}_{\Pi_j} = \int \mathbf{B}^T(\mathbf{C}\tilde{\mathbf{B}}_{\Pi_j}\mathbf{d} - \sigma div(\Pi_j))d\Omega + \int \tilde{\mathbf{B}}^T_{\Pi_j}\sigma d\Omega, \tag{12}$$

where $\mathbf{C}$ is the linear elastic constitutive matrix. The matrix $\tilde{\mathbf{B}}_{\Pi_j}$ is assembled similar to the construction of the $\mathbf{B}$ matrix. Each component of $\tilde{\mathbf{B}}_{\Pi_j}$ is constructed by multiplying the gradient of the function Π. Details can be found in (41). The virtual displacement field $\tilde{\mathbf{d}}_j$ is given by

$$\tilde{\mathbf{d}}_j = \mathbf{K}^{-1}\tilde{\mathbf{f}}_{\Pi_j}. \tag{13}$$

The derivative of the energy release rate at fracture tip i corresponding to incremental of fracture tip j increment is computed using

$$\frac{\partial G_i}{\partial l_j} = \mathbf{d}^T[\int(\mathbf{B}^T\mathbf{C}\tilde{\mathbf{B}}_{\Theta_i} + \int \tilde{\mathbf{B}}^T_{\Theta_i}\mathbf{C}\mathbf{B} - \mathbf{B}^T\mathbf{C}\mathbf{B})d\Omega]\tilde{\mathbf{d}}^T_j. \tag{14}$$

The construction of $\tilde{\mathbf{B}}_{\Theta_i}$ is carried out by multiplying $\mathbf{B}$ with the gradient of the function Θ. As mentioned above, the gradients of both function Π and function Θ are involved in the entire process to construct the matrix $\partial G/\partial l$. The gradients of these two functions are both 0 outside the colored zone in Fig. 3 . Therefore this construction process is only needed on colored zones.
The matrix $\partial G/\partial l$ is constructed by assembling the terms $\partial G_i/\partial l_j$. The maximum subdeterminant of matrix $\partial G/\partial l$ provides the set of fracture tips that would grow in the current time step, defined as N_{act}, which read

$$N_{act} = \underbrace{max}_{\forall i,j \in n_{comp}} \left[det(\frac{\partial G_i}{\partial l_j}) \geqslant 0\right]. \tag{15}$$

iMS-XFEM in Simulation of Multiple Fractures Propagation

The propagation of a fracture network, unlike propagation of a single fracture, means that much more extra DOFs are added in each new time step. Multiscale simulation becomes necessary to reduce the computational burden due to excessive number of fractures. MS-XFEM, as described in (47) is creating a finite element type system on a coarse scale mesh without any extra DOFs required. It would become a good solution to simulate the fractures propagation in underground formation. Iterative MS-XFEM can control the error level in the final solution as will be explained.

Multiscale Extended Finite Element Method (MS-XFEM)

The fine scale solution $\mathbf{d}^h$ can be approximated with the solution field $\mathbf{d}'^h$ by a multiscale formulation

$$\mathbf{d}^h \approx \mathbf{d}'^h = \mathbf{P}\,\mathbf{d}^H, \tag{16}$$

where $\mathbf{P}$ is the matrix of basis functions (i.e., prolongation operator) and $\mathbf{d}^H$ are the coarse-scale nodal displacements at the coarse scale mesh Ω^H. All extra DOFs and enrichment functions are included in matrix $\mathbf{P}$ instead of vector $\mathbf{d}^H$, which reduces the size of the coarse scale linear system. This is crucial in significantly improving the computational efficiency in these large-scale heterogeneous systems.
MS-XFEM solves the linear system of equations on the coarse mesh, imposed on a given fine-scale mesh, as shown in Fig. 4. The coarsening ratio is defined as the ratio between the coarse mesh size and fine-scale mesh size, which is 4×4 for the example shown in Fig. 4.

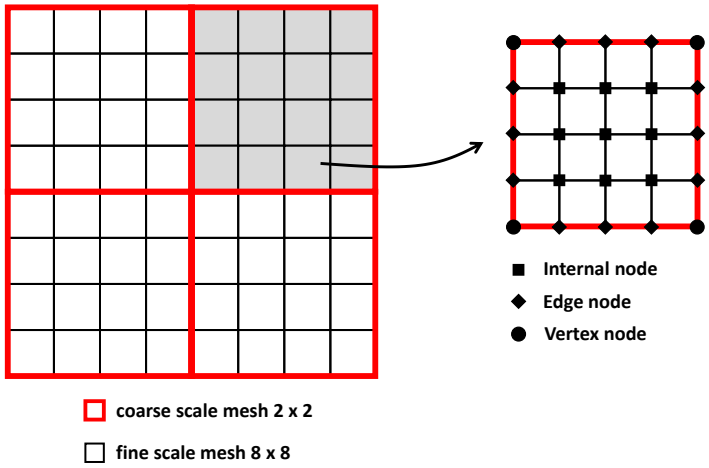

Figure 4: Illustration of the multiscale mesh imposed on a given fine-scale mesh, with a coarsening ratio of 4×4. In each coarse element there are three types of nodes: internal nodes, edge nodes and vertex nodes.

To construct the coarse-scale system of equations and solve for $\mathbf{d}^H$, the fine-scale linear system($\mathbf{K}^h\ \mathbf{d}^h = \mathbf{f}^h$) is restricted to the coarse-scale via

$$\underbrace{(\mathbf{R}\ \mathbf{K}^h\ \mathbf{P})}_{\mathbf{K}^H}\ \mathbf{d}^H = \mathbf{R}\ \mathbf{f}^h. \tag{17}$$

Here, $\mathbf{R}$ is the restriction operator with size $N^H \times N^{h+j+c}$, defined as the transpose of basis function operator

$$\mathbf{R} = \mathbf{P}^T, \tag{18}$$

where N^{h+j+c} is the size of the fine-scale enriched XFEM system including the extra DOFs and N^H is the size of coarse mesh. Prolongation operator $\mathbf{P}$ has the dimension of $N^{h+j+c} \times N^H$. This results in the coarse-scale system matrix $\mathbf{K}^H$ size of $N^H \times N^H$.
Once the coarse-scale system is solved on $\mathbf{K}^H$ space for $\mathbf{d}^H$, one can compute the approximate fine-scale solution using Eq. (16). Overall, the multiscale procedure can be summarised as finding an approximate solution $\mathbf{d}'^h$ according to

$$\mathbf{d}^h \approx \mathbf{d}'^h = \mathbf{P}\ \mathbf{d}^H = \mathbf{P}(\mathbf{R}\ \mathbf{K}^h\ \mathbf{P})^{-1}\mathbf{R}\ \mathbf{f}^h. \tag{19}$$

In here, the term $\mathbf{P}(\mathbf{R}\ \mathbf{K}^h\ \mathbf{P})^{-1}\mathbf{R}$ is called the multiscale operator $\mathbf{M}_{\mathbf{MS}}^{-\mathbf{1}}$.
Next, the prolongation operator $\mathbf{P}$, i.e., the basis functions are explained in detail. Once $\mathbf{P}$ is known, all terms in Eq. (19) are defined.
In order to construct the basis functions, the algebraic method is one convenient method. In Fig. 4, it is shown that all nodes in any coarse element can be split into three groups: internal, edge and vertex nodes.
The coarse-scale solution can be computed based on the solutions on the vertex nodes. The functions that interpolate the solution between the vertex nodes through the edge and internal nodes are then the necessary basis functions.
To develop the basis functions, first the fine-scale stiffness matrix $\mathbf{K}^h$ is permuted using the permutation operator $\mathbf{T}$ as

$$\mathbf{K}^v = \mathbf{T}\ \mathbf{K}^h\ \mathbf{T}^T = \mathbf{T} \begin{bmatrix} K_{uu} & K_{ua} & K_{ub} \\ K_{au} & K_{aa} & K_{ab} \\ K_{bu} & K_{ba} & K_{bb} \end{bmatrix} \mathbf{T}^T = \begin{bmatrix} K_{II} & K_{IE} & K_{IV} \\ K_{EI} & K_{EE} & K_{EV} \\ K_{VI} & K_{VE} & K_{VV} \end{bmatrix}. \tag{20}$$

Here, I represents the internal nodes, E represents the edge nodes and V represents the vertex nodes. The permuted linear system, therefore, reads

$$\begin{bmatrix} K_{II} & K_{IE} & K_{IV} \\ K_{EI} & K_{EE} & K_{EV} \\ K_{VI} & K_{VE} & K_{VV} \end{bmatrix} \begin{bmatrix} d_I \\ d_E \\ d_V \end{bmatrix} = \begin{bmatrix} f_I \\ f_E \\ f_V \end{bmatrix}. \tag{21}$$

Note that the permuted system collects all entries of the XFEM discrete system belonging to I, E, and V nodes.
A reduced-dimensional boundary condition is imposed as localization condition. This causes the entry K_{EI} to vanish, as the connectivity between the edge and internal nodes for the edge elements is assumed to disappear. Since the solution at vertex nodes will be obtained from the coarse-scale system, the reordered fine-scale matrix can now be reduced to

$$\begin{bmatrix} K_{II} & K_{IE} & K_{IV} \\ 0 & K^R_{EE} & K^R_{EV} \\ 0 & 0 & K^H \end{bmatrix} \begin{bmatrix} d'_I \\ d'_E \\ d'_V \end{bmatrix} = \begin{bmatrix} 0 \\ 0 \\ f^H \end{bmatrix}. \tag{22}$$

Given the solution at the coarse nodes d'_V, one can obtain the solution at the edge via

$$d'_E = -(K^R_{EE})^{-1} K^R_{EV}\, d'_V = \mathbf{P}_E\, d'_V. \tag{23}$$

The solution at the internal nodes is then obtained by solving 2D local XFEM problems subject to Dirichlet condition defined by the solutions at boundary and vertex nodes.
The prolongation matrix is finally defined as

$$\mathbf{d}' = \begin{bmatrix} d'_I \\ d'_E \\ d'_V \end{bmatrix} = \underbrace{\begin{bmatrix} -K_{II}^{-1}(-K_{IE}(K^R_{EE})^{-1}K^R_{EV} + K_{IV}) \\ -(K^R_{EE})^{-1}K^R_{EV} \\ I_{VV} \end{bmatrix}}_{\mathbf{P}} d'_V. \tag{24}$$

Here, I_{VV} is the diagonal identity matrix equal to the size of the number of vertex nodes.
After defining the prolongation operator algebraically, based on the entries of the 2D XFEM (for internal nodes) and 1D XFEM (for edge nodes), one can determine the multiscale solution.

Iterative multiscale extended finite element method (iMS-XFEM)

Preconditioned GMRES is applied to control the error and reduce it to any desired tolerance. The iterative strategy is introduced in detail in (22; 47) to improve accuracy. To reduce the high frequency error, a fine-scale smoother $\mathbf{M}^{-1}_{sm}$ (usually named as ILU(0) (11)) is paired with the multiscale operator $\mathbf{M}^{-1}_{MS}$. The preconditioner used here involves the multiscale operator and the fine scale smoothing operator following

$$\mathbf{M}^{-1} = \mathbf{M}^{-1}_{MS} + \mathbf{M}^{-1}_{sm}(I - K_f\, \mathbf{M}^{-1}_{MS}). \tag{25}$$

iMS-XFEM on fracture propagation

Propagation of crack tips can be simulated using iMS-XFEM. Crack tip growth results in new enriched elements and thus change the fine scale stiffness matrix. In terms of the multiscale method, this fine scale crack propagation is mainly affecting the basis functions since it captures all the fine scale discontinuities. If the basis functions can be updated during each crack growth step, the fine scale fracture propagation can be simulated using the iMS-XFEM. One example of updating the basis functions are shown in the test case.

Numerical Test Cases

In this section several test cases have been performed to investigate the applicability of the iMS-XFEM in simulation of single and multiple fractures propagation. These test cases are simulated using the iMS-XFEM and compared with the fine scale results to check accuracy. In the following test cases, the material is homogeneous sandstone with a Young's modulus $E = 25GPa$ and Poisson's ratio of 0.2. The fracture toughness of sandstone $K_c = 1.4 \times 10^6 Pa \cdot m^{-\frac{1}{2}}$.
Preconditioned GMRES is used to control the accuracy of the results. The criterion to stop the iterations is set as if the norm of the residual $||r^n||_2$ at current time step t^n is less than τ of the original residual norm $||r^0||_2$

$$\frac{||r^n||_2}{||r^0||_2} \leqslant \tau. \tag{26}$$

The tolerance input is affecting the number of iterations required to reach convergence. In here, the result obtained without iterative strategy and two other tolerance values, $\tau = 10^{-8}$ and $\tau = 10^{-2}$, are applied. Normally there is no doubt that a tolerance of $\tau = 10^{-8}$ would give very accurate iMS-XFEM solutions but it is also valuable to analyze whether the less accurate solutions ($\tau = 10^{-2}$) are acceptable since this less accurate solution has less computational burden.

Test case 1: homogeneous sandstone with multiple fractures

In the first test case, a square 2D domain of $L \times L$ with $L = 10$[m] is considered. The fine-scale mesh consists of 49×49 elements, while the coarse scale mesh contains only a 7×7 coarse grid. This results in a coarsening ratio of 7×7 in both x and y directions. The fractures setup is shown in Fig. 5. The fractures are located around its center point with coordinates shown in brackets. The two fractures have been labeled with a number from 1 to 2. The initial length of each fracture are both 2 [m]. The angle shown also in the bracket in Fig. 5 is the angle of fracture inclined around its center point. The number of maximum growing step sizes is set as 18 [s] and each time step size is 1 [s]. The fracture increment is set as 0.4 [m]. The Dirichlet boundary conditions are applied at the bottom. At the top a distributed

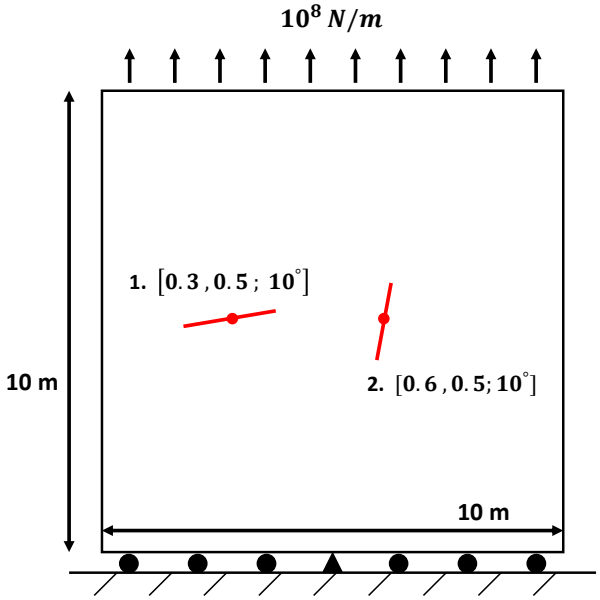

Figure 5: Test case 1: Multiple fractures within a homogeneous sandstone reservoir under tension stress.

In the following, only the test with an iterative strategy and tolerance of $\tau = 10^{-2}$ is studied. The propagating crack path at step 4 and 12 are shown in Fig. 6 in the left column. Red color segments represent the fracture pattern predicted using iMS-XFEM solution and blue segments represent the fracture pattern predicted using only fine scale XFEM solution. It is clear that not all tips will grow considering the global minimum energy release by Eq. (15). The stress plots are shown in the middle column, which partly reveals why some tips grow and others do not. The corresponding displacement fields at these steps are plotted in the right column. The red lines represent the coarse scale mesh with iMS-XFEM displacement result plotted on coarse scale grids. The blue lines represent the fine scale displacement result.
The sequence of propagating crack tips is as follows. First, the left tip of fracture 1 grows to the left edge since that the maximum stress is located around the left tip of fracture 1, as shown in Fig. 6 (b). At step 5, the left tip of fracture 1 reaches at the left edge of domain. Then the right tip of fracture 1 propagates. At step 12, the right fracture tip of fracture 1 joins fracture 2. The crossing point is also where the peak stress locate around as shown in Fig. 6 (e). The top fracture tip of fracture 2 continues to grow to the right edge.

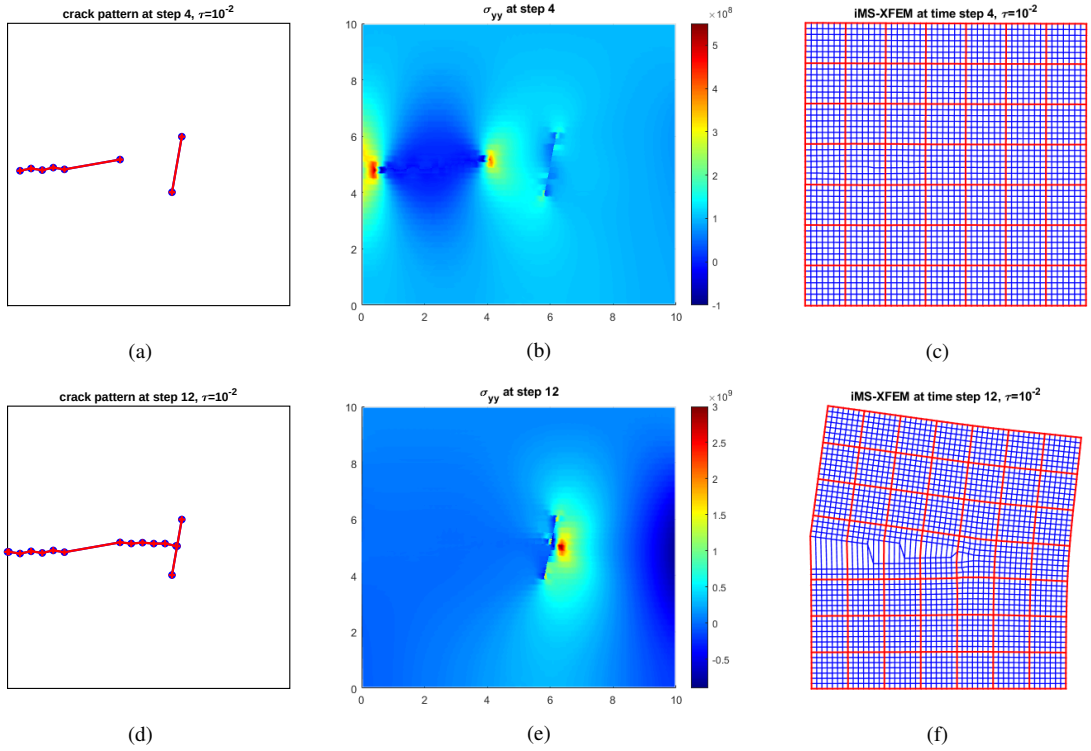

Figure 6: Test case 1: crack paths growing history at step 4 and 12. Left column includes crack patterns predicted. Red segments and crosses represent crack paths predicted using iMS-XFEM result and blue segments and circles represent the crack paths predicted using fine scale XFEM result. The middle column includes the stress plot of σ_{yy} at these steps. The right column includes the corresponding displacement fields at these steps. Blue lines represent the fine scale XFEM result while red lines represent the iMS-XFEM results and the coarse scale grid.

The convergence characteristics recorded using preconditioned GMRES are shown in Fig. 7. In this figure, the convergence at step 4 and 12 have been plotted. The number of extra DOFs for each of these steps is: 118 and 176. The iterations required to reach convergence with respect to tolerance of 10^{-8} are: 28 and 39, respectively. Still the number of iterations required to reach convergence is increasing as the fracture is growing. It can be approximately stated that the number of iterations to reach convergence is growing proportionally by the increase of DOFs. It is noted that the convergence behavior for step 12 is not good as the residual is not reduced significantly in the first 5 iterations. This is mainly due to the

extreme displacement field as shown Fig. 6 (f). This kind of extreme displacement field is not usual in geological formations deformation.

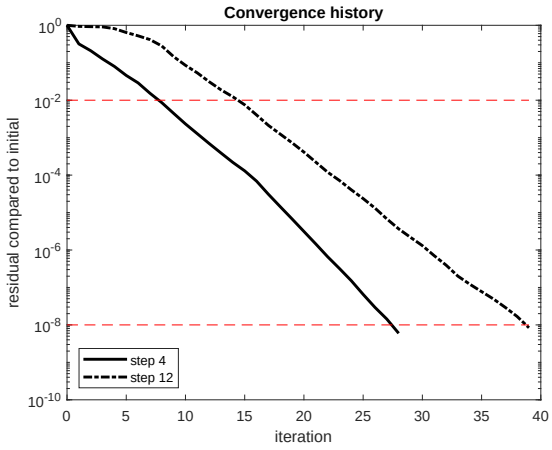

Figure 7: Test case 1: convergence history using preconditioned GMRES. The number of extra DOFs for each of these steps are: 118 and 176. The number of iterations to reach convergence is increasing with the growth of fractures.

Conclusion

An iterative multiscale method for XFEM, namely iMS-XFEM, is proposed to track the growth of multiple fractures in underground formations. The growth of fractures leads to the extension and also the junction of the discontinuities. The basis functions are capable of capturing this extension or junction of the fine scale fractures. The basis functions are updated in an algebraic manner based on the fine-scale stiffness matrix, which is revised in accordance with the growth of fractures. This makes iMS-XFEM suitable to simulate propagation of fractures. A test case result shows that iMS-XFEM with preconditioned GMRES track the growth of fractures paths correctly, even if the error tolerance is not that extreme. This means that the basis functions successfully capture the changes of these fractures. This is promising for iMS-XFEM's further application into for example 3D complicated highly fractured formations simulation which is the most suitable model for natural fractured formations.

Acknowledgments

Fanxiang Xu is sponsored by the Chinese Scholarship Council (CSC). Authors acknowledge all members of the Delft Advanced Reservoir Simulation (DARSim) group, ADMIRE research group and computational mechanics group. Special thanks to Dr. N. Castelletto and Prof. C. Vuik for their valuable discussions and suggestions.

References

[1] Abdulle, A. and Weinan, E. [2003] Finite difference heterogeneous multi-scale method for homogenization problems. *Journal of Computational Physics*, **191**(1), 18–39.
[2] Allaire, G. [1992] Homogenization and two-scale convergence. *SIAM Journal on Mathematical Analysis*, **23**(6), 1482–1518.
[3] Amanbek, Y., Singh, G., Wheeler, M.F. and van Duijn, H. [2019] Adaptive numerical homogenization for upscaling single phase flow and transport. *Journal of Computational Physics*, **387**, 117–133.
[4] Aragón, A.M. and Simone, A. [2017] The Discontinuity-Enriched Finite Element Method. *International Journal for Numerical Methods in Engineering*, **112**(11), 1589–1613.
[5] Belytschko, T. and Black, T. [1999] Elastic crack growth in finite elements with minimal remeshing. *International Journal for Numerical Methods in Engineering*, **45**(5), 601–620.
[6] Belytschko, T., Lu, Y.Y. and Gu, L. [1994] Element-free Galerkin methods. *International Journal for Numerical Methods in Engineering*, **37**(2), 229–256.
[7] Bittencourt, T., Wawrzynek, P., Ingraffea, A. and Sousa, J. [1996] Quasi-automatic simulation of crack progation for 2D LEFM problems. *Engineering Fracture Mechanics*, **55**, 321–334.
[8] Budyn, É., Zi, G., Moës, N. and Belytschko, T. [2004] A method for multiple crack growth in brittle materials without remeshing. *International Journal for Numerical Methods in Engineering*, **61**(10), 1741–1770.
[9] Castelletto, N., Hajibeygi, H. and Tchelepi, H. [2016] Hybrid Multiscale Formulation for Coupled Flow and Geomechanics. In: *ECMOR XV - 15th European Conference on the Mathematics of Oil Recovery*. EAGE Publications BV.
[10] Castelletto, N., Hajibeygi, H. and Tchelepi, H.A. [2017] Multiscale finite-element method for linear elastic geomechanics. *Journal of Computational Physics*, **331**, 337–356.
[11] Chow, E. and Saad, Y. [1997] Experimental study of ILU preconditioners for indefinite matrices. *Journal of Computational and Applied Mathematics*, **86**(2), 387–414.
[12] Chung, E.T., Efendiev, Y. and Li, G. [2014] An adaptive GMsFEM for high-contrast flow problems. *Journal of Computational Physics*, **273**, 54 – 76.
[13] Daux, C., Moës, N., Dolbow, J., Sukumar, N. and Belytschko, T. [2000] Arbitrary branched and intersecting cracks with the extended finite element method. *International journal for numerical methods in engineering*, **48**(12), 1741–1760.
[14] Deb, R. and Jenny, P. [2017] Finite volume-based modeling of flow-induced shear failure along fracture manifolds. *International Journal for Numerical and Analytical Methods in Geomechanics*, **41**(18), 1922–1942.
[15] Efendiev, Y., Galvis, J., Li, G. and Presho, M. [2014] GENERALIZED MULTISCALE FINITE ELEMENT METHODS: OVERSAMPLING STRATEGIES. *International Journal for Multiscale Computational Engineering*, **12**(6), 465–484.
[16] Erdogan, F. and Sih, G.C. [1963] On the Crack Extension in Plates Under Plane Loading and Transverse Shear. *Journal of Basic Engineering*, **85**(4), 519–525.
[17] Fumagalli, A. and Scotti, A. [2014] An Efficient XFEM Approximation of Darcy Flows in Arbitrarily Fractured Porous Media. *Oil & Gas Science and Technology – Revue d'IFP Energies nouvelles*, **69**(4), 555–564.
[18] Garipov, T.T., Tomin, P., Rin, R., Voskov, D.V. and Tchelepi, H.A. [2018] Unified thermo-compositional-mechanical framework for reservoir simulation. *Computational Geosciences*, **22**(4), 1039–1057.
[19] Giovanardi, B., Formaggia, L., Scotti, A. and Zunino, P. [2017] Unfitted FEM for Modelling the Interaction of Multiple Fractures in a Poroelastic Medium. In: *Lecture Notes in Computational Science and Engineering*, Springer International Publishing, 331–352.
[20] Griffith, A.A. [1921] VI. The phenomena of rupture and flow in solids. *Philosophical Transactions of the Royal Society of London. Series A, Containing Papers of a Mathematical or Physical Character*, **221**(582-593), 163–198.
[21] Hajiabadi, M.R. and Khoei, A.R. [2018] A bridge between dual porosity and multiscale models of heterogeneous deformable porous media. *International Journal for Numerical and Analytical Methods in Geomechanics*, **43**(1), 212–238.
[22] Hajibeygi, H., Bonfigli, G., Hesse, M.A. and Jenny, P. [2008] Iterative multiscale finite-volume

method. *Journal of Computational Physics*, **227**(19), 8604–8621.
[23] Hajibeygi, H. and Jenny, P. [2009] Multiscale finite-volume method for parabolic problems arising from compressible multiphase flow in porous media. *Journal of Computational Physics*, **228**(14), 5129–5147.
[24] Hajibeygi, H., Karvounis, D. and Jenny, P. [2011] A hierarchical fracture model for the iterative multiscale finite volume method. *J. Comput. Phys.*, **230**, 8729–8743.
[25] Hornung, U. [1997] *Homogenization and Porous Media*, 6. Springer Science & Business Media.
[26] Jenny, P., Lee, S. and Tchelepi, H. [2003] Multi-scale finite-volume method for elliptic problems in subsurface flow simulation. *Journal of Computational Physics*, **187**(1), 47–67.
[27] Jiang, J. and Younis, R.M. [2016] Hybrid Coupled Discrete-Fracture/Matrix and Multicontinuum Models for Unconventional-Reservoir Simulation. *SPE J.*, **21**, 1009–1027.
[28] Khoei, A. and Hajiabadi, M. [2018] Fully coupled hydromechanical multiscale model with micro-dynamic effects. *International Journal for Numerical Methods in Engineering*, **115**(3), 293–327.
[29] Khoei, A.R., Vahab, M., Haghighat, E. and Moallemi, S. [2014] A mesh-independent finite element formulation for modeling crack growth in saturated porous media based on an enriched-FEM technique. *International Journal of Fracture*, **188**(1), 79–108.
[30] Kumar, K., van Noorden, T. and Pop, I.S. [2014] Upscaling of reactive flows in domains with moving oscillating boundaries. *Discrete & Continuous Dynamical Systems*, **7**, 623–644.
[31] Meer, F.P. and Sluys, L.J. [2009] A phantom node formulation with mixed mode cohesive law for splitting in laminates. *International Journal of Fracture*, **158**(2), 107–124.
[32] Melenk, J. and Babuška, I. [1996] The partition of unity finite element method: Basic theory and applications. *Computer Methods in Applied Mechanics and Engineering*, **139**(1), 289 – 314.
[33] Moes, N., Dolbow, J. and Belytschko, T. [1999] A finite element method for crack growth without remeshing. *International Journal for Numerical Methods in Engineering*, **46**(1), 131–150.
[34] Osher, S. and Sethian, J.A. [1988] Fronts propagating with curvature-dependent speed: Algorithms based on Hamilton-Jacobi formulations. *Journal of Computational Physics*, **79**(1), 12–49.
[35] Patil, R., Mishra, B. and Singh, I. [2017] A new multiscale XFEM for the elastic properties evaluation of heterogeneous materials. *International Journal of Mechanical Sciences*, **122**, 277–287.
[36] Rashid, M. [1998] The arbitrary local mesh replacement method: An alternative to remeshing for crack propagation analysis. *Computer Methods in Applied Mechanics and Engineering*, **154**(1-2), 133–150.
[37] Ren, G., Jiang, J. and Younis, R.M. [2016] A Fully Coupled XFEM-EDFM Model for Multiphase Flow and Geomechanics in Fractured Tight Gas Reservoirs. *Procedia Computer Science*, **80**, 1404–1415.
[38] Rice, J.R. [1968] A Path Independent Integral and the Approximate Analysis of Strain Concentration by Notches and Cracks. *Journal of Applied Mechanics*, **35**(2), 379–386.
[39] Sokolova, I., Bastisya, M.G. and Hajibeygi, H. [2019] Multiscale finite volume method for finite-volume-based simulation of poroelasticity. *Journal of Computational Physics*, **379**, 309–324.
[40] Stolarska, M., Chopp, D.L., Moës, N. and Belytschko, T. [2001] Modelling crack growth by level sets in the extended finite element method. *International Journal for Numerical Methods in Engineering*, **51**(8), 943–960.
[41] Suo, X.Z. and Combescure, A. [1992] Double virtual crack extension method for crack growth stability assessment. *International journal of fracture*, **57**(2), 127–150.
[42] Tene, M., Bosma, S.B., Kobaisi, M.S.A. and Hajibeygi, H. [2017] Projection-based Embedded Discrete Fracture Model (pEDFM). *Advances in Water Resources*, **105**, 205–216.
[43] Wang, Y., Hajibeygi, H. and Tchelepi, H.A. [2014] Algebraic multiscale solver for flow in heterogeneous porous media. *Journal of Computational Physics*, **259**, 284 – 303.
[44] Wang, Y. and Shahvali, M. [2016] Discrete fracture modeling using Centroidal Voronoi grid for simulation of shale gas plays with coupled nonlinear physics. *Fuel*, **163**, 65–73.
[45] Wu, C.H. [1978] Maximum-energy-release-rate criterion applied to a tension-compression specimen with crack. *Journal of Elasticity*, **8**(3), 235–257.
[46] Wu, J.Y. and Li, F. [2015] An improved stable XFEM (Is-XFEM) with a novel enrichment function for the computational modeling of cohesive cracks. *Computer Methods in Applied Mechanics and Engineering*, **295**, 77–107.
[47] Xu, F., Hajibeygi, H. and Sluys, L.J. [2021] Multiscale extended finite element method for deformable fractured porous media. *Journal of Computational Physics*, **436**, 110287.

[48] Zhang, H.W., Wu, J.K., Lü, J. and Fu, Z.D. [2010] Extended multiscale finite element method for mechanical analysis of heterogeneous materials. *Acta Mechanica Sinica*, **26**(6), 899–920.